Laser Calibration for Powder Bed Fusion Additive Manufacturing Process

Ho Yeung, Steven Grantham

National Institute of Standards and Technology (NIST), Gaithersburg, MD 20899

Abstract

Laser powder bed fusion systems use a high-power laser, steered by two galvanometer mirrors to scan a pattern on metal powder layers. The laser spot size, position, and synchronization between the laser power and position are critical to the build quality. This paper describes in-situ calibration techniques utilizing a digital camera to image the attenuated laser beam directly. The laser spot size is measured using laser beam images taken by the camera at different heights. The laser position measurement involves commanding the galvanometer motor to scan through a grid of points on the camera sensor. The synchronization of laser power and position is verified by observing the intersections of the adjacent scan vectors. These methods provide not only a tool for calibration but also insights into the laser control for the laser powder bed fusion additive manufacturing process.

Introduction

Additive manufacturing (AM) technology has evolved from its early use in prototyping to part fabrication in many industries, including aerospace, medical, and automotive. It is very useful for creating parts that are too difficult to manufacture traditionally. One type of AM process is laser powder bed fusion (LPBF) [1], where a high-energy laser beam is projected to the build plane by a pair of mirrors driven by galvanometer (galvo) motors, to selectively fuse a thin layer of metal powder into cross-sections of the intended three-dimensional structure. This process is repeated after each successive layer of metal powder is spread on top of the completed layer, until the three-dimensional structure is completed.

Figure 1 shows a simplified schematic of LPBF laser control, where the angular position θ of the mirror/galvo motor is translated into linear displacement of the laser beam on the build plane. Since there is no practical way to measure the laser position on the build plane during the build, the laser position control is an open loop. Therefore, position calibration is important for part dimension accuracy. There are different methods [2–4] for laser position calibration; the most common one is the "mark and measure" [2, 3], where a pattern is burned on a metal plate and measured by coordinate measuring machine (CMM), and compared with the programmed path. The accuracy of this method is on the order of 20 μm [3].

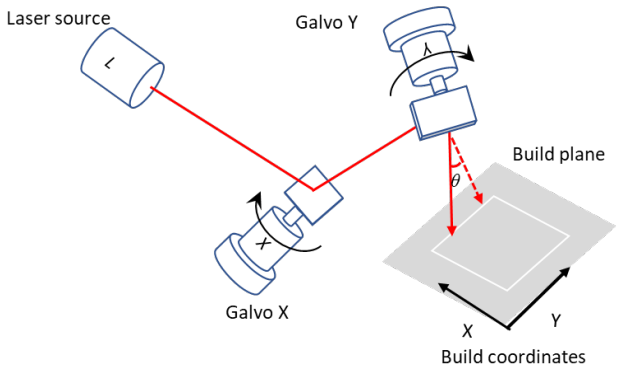

Figure 1. Simplified schematic for LPBF laser control.

To build high-quality parts, the laser power needs to be fully synchronized with the laser position. The synchronization error can be caused by a delay error and/or the following error. This is explained in Figure 2, where a circle is scanned. Figure 2a shows the ideal (programmed) path/power. Since the laser response is much faster than the galvo, a delay time needs to be inserted into the laser command. Figure 2b shows a case when this delay time is set longer than it should be, and the laser is not turned on/off at the boundary. Following error happens when the programmed path/speed requires higher acceleration than the system can deliver. Figure 2c shows an example where the galvo is not fast enough to execute the command, and the scan path cannot reach the boundary. It is believed that synchronization issues are a major cause of the subsurface pores sometimes found in additively manufactured parts [5].

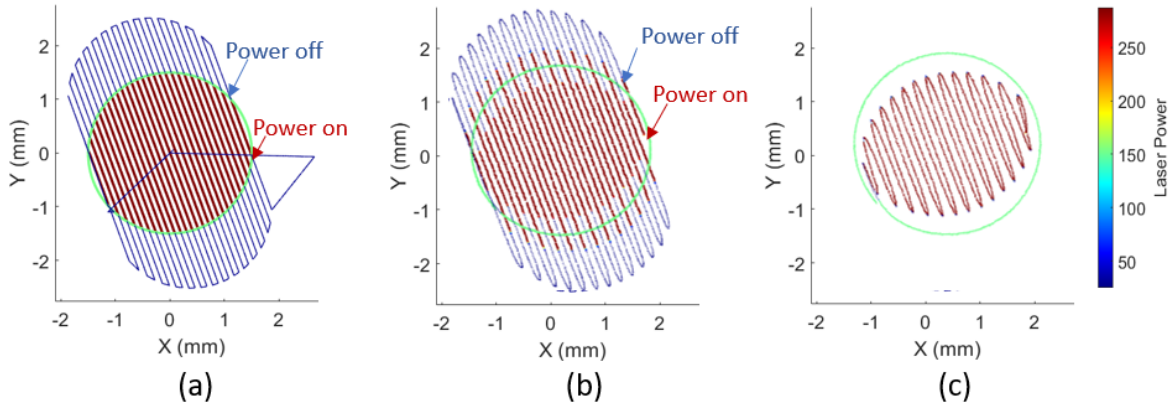

Figure 2. Laser power plots show infill hatch lines for a circle [5]. (a) The programmed (ideal) path/power. (b) Delay error. (c) Following error.

It is commonly known that laser beam shape, profile, and size are important to the build process. If the laser spot size is too big, the energy density may be too low to fully melt the powder. Lack of fusion defects may occur [6]. If the laser spot size is too small, it could cause keyholing [7]. Therefore, laser calibrations are needed to make sure (1) laser position is accurate, (2) laser beam size and shape are accurate and correctly compensated, and (3) laser position and power are synchronized. In this paper, we describe how to build a simple calibration setup with very low-cost components to conduct the above calibrations.

LPBF laser calibration setup

The calibration methods proposed here utilize a low-cost complementary metal-oxide semiconductor (CMOS) camera to directly image the attenuated laser beam of an AM machine. Figure 3 shows a schematic of the calibration setup, where a camera is positioned in parallel to the build plane (X-Y plane) and looks up the laser beam. The camera used here is a Basler daA2500-14um[1], but any camera with similar specifications should work. The camera specification is given in Table 1. The camera has a frame rate of 14 fps; the calibration methods proposed here do not require a high-speed camera.

Table 1. Camera specification

Resolution	2592 pixel x 1944 pixel
CMOS Size	5.7 mm x 4.3 mm
Pixel Size	2.2 µm x 2.2 µm
Frame Rate	14 fps
Image	12-bit monochrome

To image the laser beam directly, the laser power must be attenuated to protect the camera CMOS sensor. This is done by neutral density (ND) filters arranged in series (Figure 3). Optical density (OD) indicates the attenuation factor provided by an ND filter. OD is related to the transmission (T) by $T = 10^{-OD}$. Three ND filters of OD 1.0, 3.0, and 4.0 are stacked together to achieve transmission of 10^{-8}. The OD 1.0 filter is placed first in the optical chain, so it will absorb most of the heat from the laser beam. The OD 1.0 filter used here is Thorlab NENIR10A-C; it is rated for 50W/cm^2 at 1064 nm.

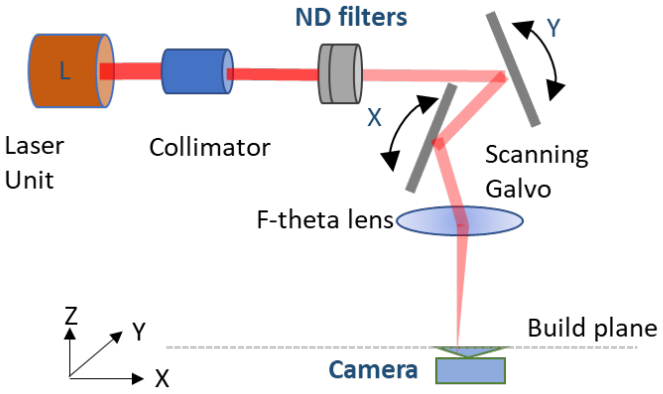

Figure 3. Laser calibration setup. A camera aligned with the build plane looks up the laser beam. The laser beam is attenuated by ND filters inserted between the collimator and scanning mirrors.

[1] Certain commercial equipment, instruments, or materials are identified in this paper in order to specify the experimental procedure adequately. Such identification is not intended to imply recommendation or endorsement by the National Institute of Standards and Technology (NIST), nor is it intended to imply that the materials or equipment identified are necessarily the best available for the purpose.

Therefore, the only hardware requirement for the calibration setup is a CMOS camera and ND filters. The camera can be mounted on the build plane with a simple fixture. The ND filters can be inserted anywhere along the laser optical path before the galvo and focusing lens. The experiments in this study are conducted on a testbed implemented with the open platform control framework [8]. The scan path is programmed in the Simple AM (SAM) control software [8]. All experiments are implemented with standard functions/features on the testbed/software. However, it is recognized that some of these implementations may not be straightforward on systems without open access.

Laser spot size calibration

On a LPBF system, the laser spot size depends on where the focused laser beam intersects with the build plane. Theoretically, the laser spot size is the smallest when the build plane is at the focal plane of the F-theta lens (Figure 3). Moving the build plane/camera away from the focal plane in either direction will increase the laser spot size.

An experiment is designed to measure the laser spot size at different build plane heights. The laser power is set at 200 W but pulsed at 5 Hz, with a pulse width of 250 μs (duty cycle = 1/800). Therefore, the average power is 0.25 W. Each laser pulse triggers the camera to take one image. The build plane is commanded to move through a range of height of Z = 18 mm to 27 mm, with 0.1 mm steps. For each Z value, 20 images are recorded. Figure 4a shows one sample image for each Z. The images are then fit with a two-dimensional (2D) Gaussian equation to determine the diameters along the x and y axes (Figure 4b and c). The normal 2D Gaussian equation is shown in Equation 1, where A is the amplitude, (x_0, y_0) is the center, and σ_x and σ_y are the standard deviations along the x and y axes. The laser spot diameter can be estimated by D4σ, which is four times the standard deviation of the distribution of intensity along the axis measured. The 2D Gaussian fit here is conducted with orientation angle θ by replacing x and y in equation (1) with $x_r = x*\cos(\theta) + y*\sin(\theta)$ and $y_r = x*\sin(\theta) + y*\cos(\theta)$; and the same for x_0 and y_0. The x-y coordinates with rotation angle θ are shown in Figure 4b.

$$f(x, y) = A \exp\left(-\left(\frac{(x-x_0)^2}{2\sigma_x^2} + \frac{(y-y_0)^2}{2\sigma_y^2}\right)\right) \quad (1)$$

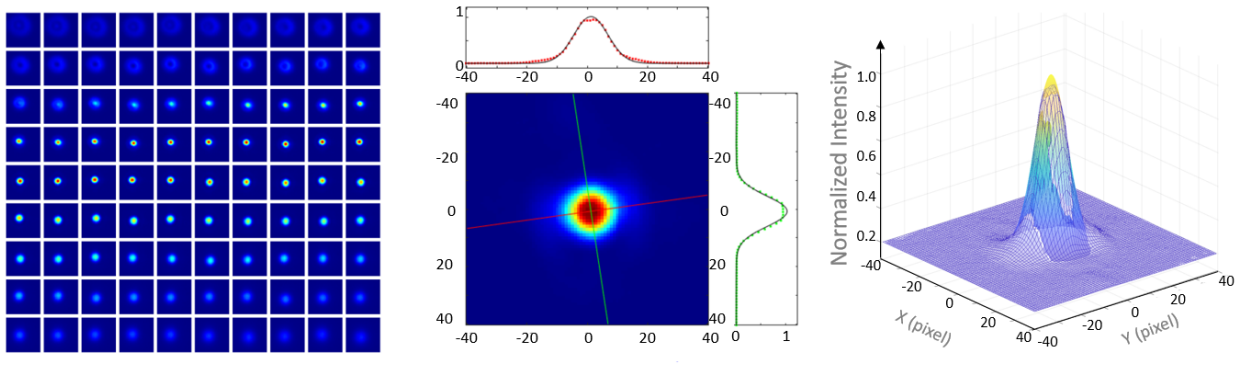

Figure 4. Laser spot size/profile calibration. (a) Laser beam images at different heights (z). From top left to bottom right, Z increases from 18.1 mm to 27.0 mm at 0.1 mm steps. (b) A sample image at Z = 22.0 mm with 2D Gaussian fit. (c) Mesh plot for 2D Gaussian fit. The pseudo color represents the image intensity.

Figure 5a plots the average laser spot sizes measured along the x-axis ($D4\sigma_x$), along the y-axis ($D4\sigma_y$), and the average of the x and y axes ($D4\sigma_{xy}$) based on the 2D Gaussian fit. The overlaps of the $D4\sigma_x$ and $D4\sigma_y$ show the laser beam is quite symmetrical. The U-shape curve can be used to set the laser spot size. For example, a 100 μm laser spot size can be obtained at both Z ≈ 26 mm and Z ≈ 20 mm, when the build plane is above or below the focal plane (Figure 5a). The distribution of laser power intensity, however, is noticeably different at these two Z values.

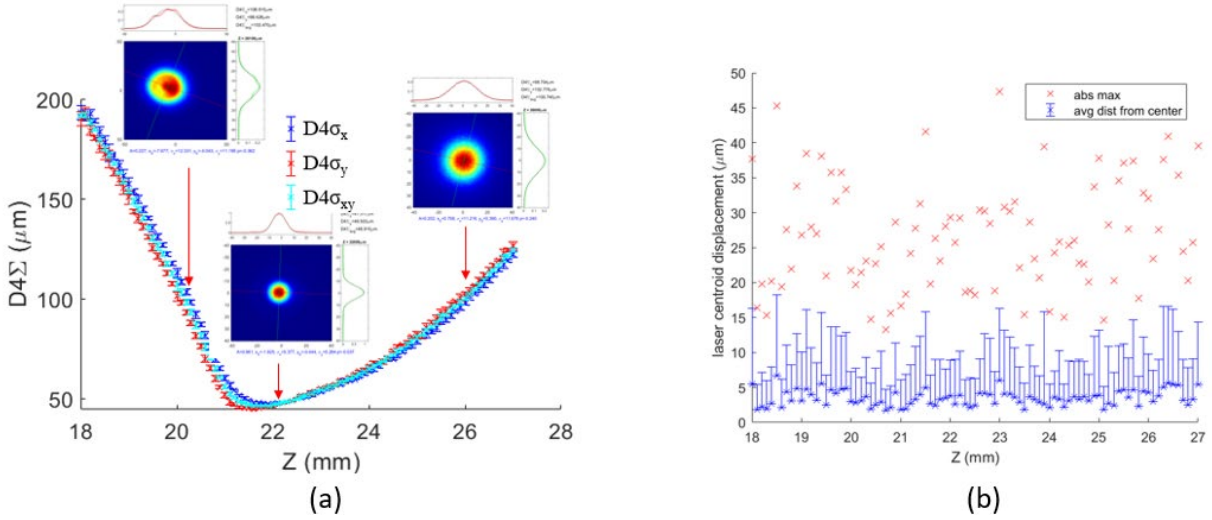

Figure 5. Laser spot size and location measurements at different build plane height Z. 20 measurements were made for each Z. The error bar shows one standard deviation. (a) Laser beam diameters based on D4σ. (b) Laser beam locations. Blue stars are the average distances from the center. Red crosses are the absolute maximum jumping distances.

The location of the laser beam can be estimated by the centroid of the laser spot in the image. The data indicate the beam location is not constant, but 'jumps' around slightly. Figure 5b plots for each Z value the average distance of the laser beam locations from their center (x_c, y_c). The center is calculated by $x_c = \sum_i^{20} x_i/20$ and $y_c = \sum_i^{20} y_i/20$, where (x_i and y_i) are the centroid coordinate of the i^{th} image. The absolute maximum (abs max) displacement is also plotted in the

figure. Abs max is calculated by the diagonal distance of the minimum rectangle inscribed by all the 20 beam locations. This jumping may be caused by mechanical vibrations, or the oscillation of the galvo motor while it is trying to hold its position. Excessive jumping may indicate a mechanical or electrical issue.

Laser position calibration

The laser position calibration utilizes the camera pixel array as a reference. The height of the four corners of the camera CMOS is checked with a laser probe to make sure it is parallel to the build plane. Assuming the camera is aligned well with the build plane and the pixel dimension is precise, the pixel array can be used to define the build coordinates. The pixel array captures the laser beam image while it is being scanned with the galvo system following a programmed path. Figure 6a shows a grid scan path designed for position calibration. The galvo is programmed to stop at each node (red dot) on the path, hold for 0.19 s; and the laser is then turned on for 200 µs. The camera is triggered 0.09 s before the laser is turned on, and the exposure time is set to 0.1 s to take one full frame image at each node. This ensures the galvo is completely settled and the camera's shutter is active before the laser beam is introduced and the image is recorded.

There are 100 nodes in the scan path shown in Figure 6a. Therefore, a total of 100 images were taken. These 100 images are superimposed into a single frame to create a laser image array as shown in Figure 6b. The positions of the laser beam image are determined by their centroid and plotted in Figure 6c, together with the corresponding commanded positions. The camera pixel array defines a build plane coordinate B (Figure 6b). The X-Y galvos define a coordinate G. The scan path is programmed in B but executed in G. A transfer function from B to G is built in the AM machine to convert the programmed laser positions to executable galvo commands. One goal of the position calibration here is to correct this transfer function to minimize the laser position error. Position error is defined as the distance between the commanded and measured positions.

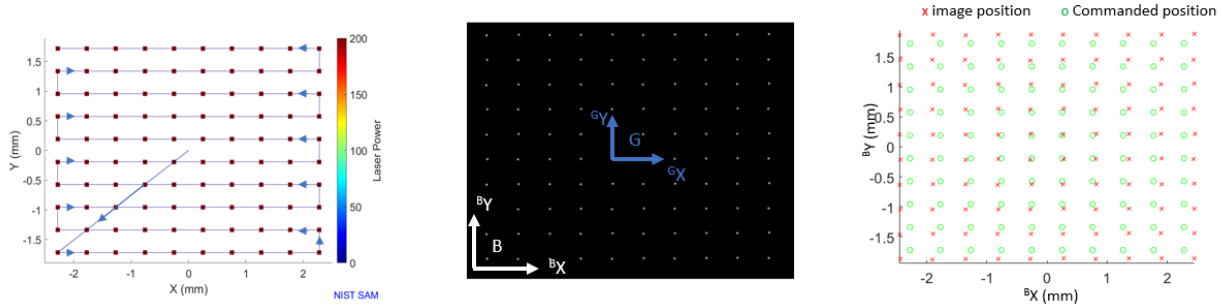

Figure 6. Laser position calibration. (a) Scan path, the laser is turned on only at the red dots. (b) Image array created by superimposing the laser beam images taken at different locations. (c) Comparison of commanded and measured positions. The laser position is determined by the centroid of the laser spot in the image.

Polynomials can be fit to map the commanded and measured positions in Figure 6c. Figure 7 shows the Matlab lab script for a third-order polynomial fit. The fitting result indicates the x and y galvos are nearly orthogonal, as all coefficients for y are very small in sfx(x, y), and

all coefficients for x are very small in sfy(x, y). The only significant coefficient is the linear part highlighted in red in Figure 7. Hence, the mapping polynomials can be approximated by the linear part only. That is, sfx(x, y) = 0.9334*x, sfy (x, y) = 0.9199*y.

```
% fit polynomial:
XYC = XY_command; XYT = XY_measured;
sfx = fit(XYT,XYC(:, 1),'poly33'); sfy = fit(XYT,XYC(:, 2),'poly33');
```

```
sfx (x,y) = p00 + p10*x + p01*y + p20*x^2 + p11*x*y + p02*y^2
          + p30*x^3 + p21*x^2*y + p12*x*y^2 + p03*y^3
   Coefficients (with 95% confidence bounds):
     p00 =   -0.002637  (-0.004358, -0.0009162)
     p10 =     0.9334  (0.9317, 0.935)
     p01 =    0.002164  (5.691e-06, 0.004323)
     p20 =   0.0001221  (-0.0003009, 0.000545)
     p11 =   0.0002049  (-0.0002841, 0.0006939)
     p02 =   0.0001836  (-0.0005452, 0.0009124)
     p30 =  -0.0003255  (-0.0006467, -4.289e-06)
     p21 =  -1.036e-05  (-0.0003654, 0.0003447)
     p12 =  -9.117e-05  (-0.0005579, 0.0003755)
     p03 =  -0.0006494  (-0.001374, 7.513e-05)
```

```
sfy (x,y) = p00 + p10*x + p01*y + p20*x^2 + p11*x*y + p02*y^2
          + p30*x^3 + p21*x^2*y + p12*x*y^2 + p03*y^3
   Coefficients (with 95% confidence bounds):
     p00 =   -0.002229  (-0.003633, -0.0008258)
     p10 =   -0.002388  (-0.003732, -0.001044)
     p01 =     0.9199  (0.9181, 0.9216)
     p20 =  -0.0001277  (-0.0004726, 0.0002173)
     p11 =   0.0003831  (-1.573e-05, 0.0007818)
     p02 =    0.000761  (0.0001666, 0.001355)
     p30 =  -0.0001309  (-0.0003929, 0.000131)
     p21 =   3.219e-05  (-0.0002573, 0.0003217)
     p12 =  -6.292e-06  (-0.0003869, 0.0003743)
     p03 =   0.0006308  (3.989e-05, 0.001222)
```

Figure 7. Matlab script (top) and the result for the polynomial fit.

A linear correction by scaling the galvo x by a factor of 0.9334 and galvo y by 0.9199 was applied. Figure 8 shows the commanded and measured laser positions after the correction. Figure 9 compares the laser position errors before and after the correction. The average error is reduced from 0.1331 mm to 0.0079 mm. Although only a linear correction is demonstrated here, a 3rd order polynomial can be applied to correct non-linear distortions from optics as well as systems where the x galvo and y galvo are not perfectly orthogonal.

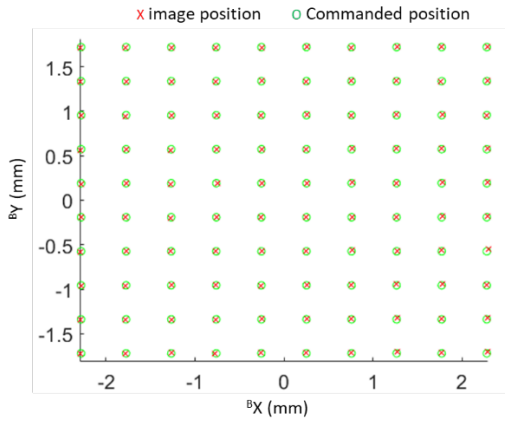

Figure 8. Position calibration after the linear correction. The measured position (image position) follows the commanded position very well.

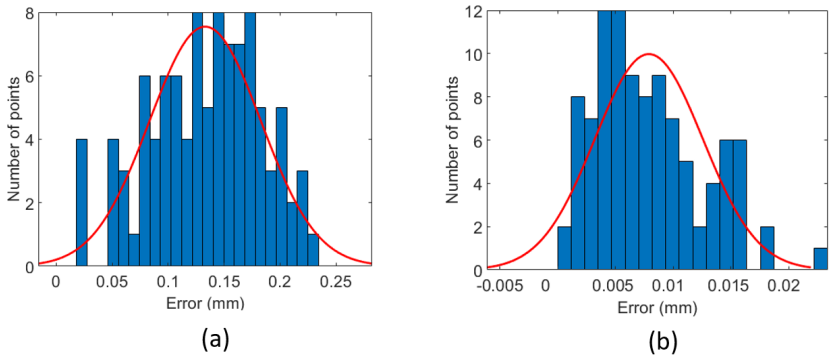

Figure 9. Laser position error distributions (a) before correction, and (b) after correction. Note the different scales on the x-axes.

The position calibration can be combined with the laser spot size calibration. The laser images in Figure 6b can also be used for the laser spot diameter measurement. The results are shown in Figure 10a. The slight increase of beam diameter in the +y direction could indicate a slightly tilted build plane or imperfectly aligned laser optics. Sample images at four corners are shown in Figure 10b and c. There is very little noticeable difference.

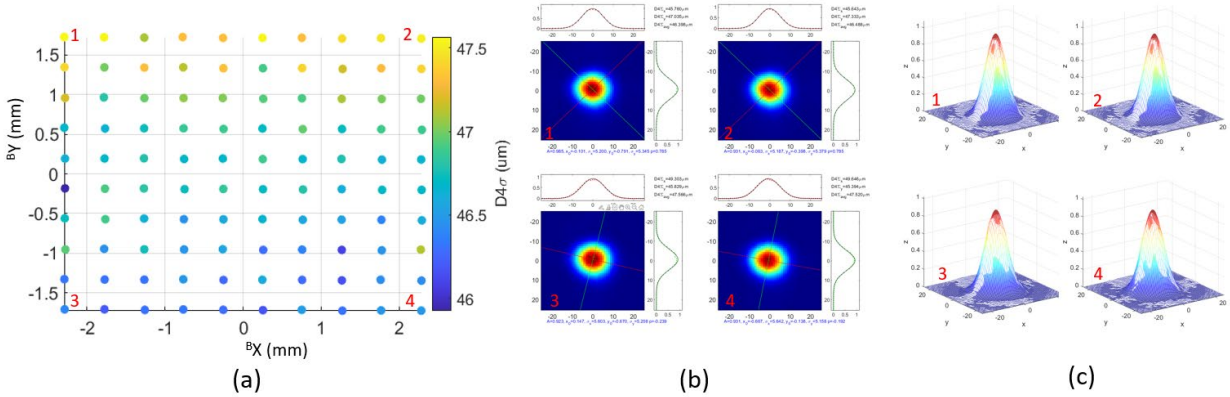

Figure 10. Laser spot size and shape calibration at different locations. (a) laser diameters at different locations. (b) Laser beam images at the four corners, labeled by 1-4. (c) 2D Gaussian fit mesh plots.

Laser synchronization calibration

To build a high-quality part, the laser needs to be switched on and off at the right place and right time during the build. An example is shown in Figure 11, where a NIST logo is scanned with a combination of three different speeds and with a constant build speed scan strategy [9]. Figure 11a plots the scan strategy, and Figure 11b shows the scan path imaged by the camera. The camera exposure is on for the complete scan. That is, a single image is taken per scan. The synchronization calibration is conducted by visually inspecting the intersections of the scan vectors. Poor synchronization will result in gaps or overruns at the intersections. At a scan speed of 1000 mm/s, for 10 µs the laser will travel 10 µm or ≈ 4.5 pixels on the camera CMOS. Since 10 µs is the temporal resolution of the galvo using the xy2-100 protocol [10], and 4 pixels difference can be

easily distinguishable in the image, the calibration method is adequate for optimizing the laser position-power synchronization under normal scan conditions.

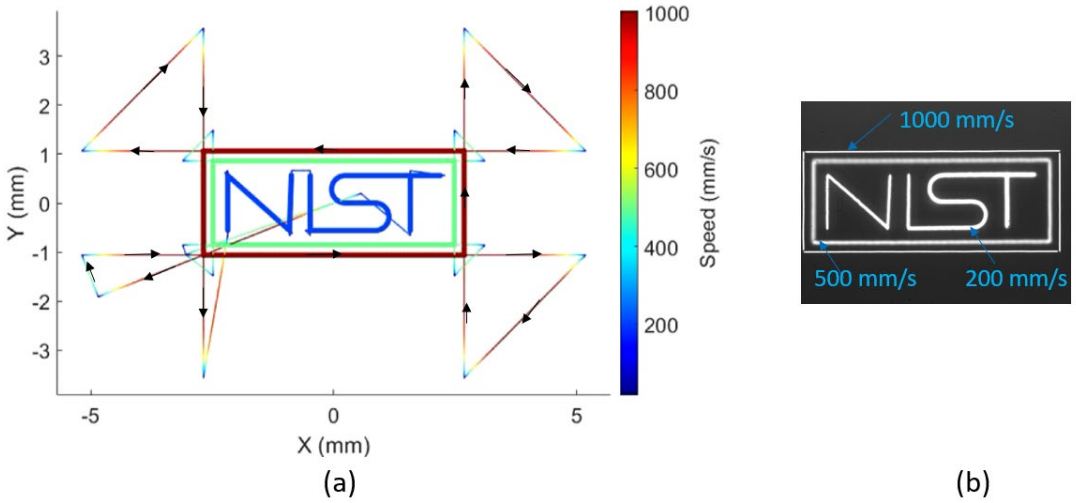

Figure 11. Image the laser scan path. (a) Programmed scan path, thick lines are where the laser power is on. (b) Laser scan path image.

Two types of synchronization errors were discussed previously and shown in Figure 2. The following error occurs when the programmed path/speed requires a higher acceleration than the system can deliver. A simple way to estimate the system acceleration is by scanning circles at different speeds and recording the resulting image. To scan a circle with radius r and speed v, the acceleration requirement is v^2/r. 49 circles of 1 mm diameter were scanned with speeds decreasing from 5000 mm/s to 200 mm/s, at 100 mm/s steps. Figure 12 shows images for 9 circles, with their scan speeds and acceleration requirements listed underneath. The distortion at higher speeds indicates the acceleration requirement cannot be met. Almost perfect circles were scanned at lower speeds. The thicker lines at lower speeds are probably due to the CMOS overflow since the scan paths overlapped more, and the power density is also higher. Figure 12 provides a quick assessment of the maximum acceleration the system can be driven without a significant following error. Most experiments in this study were programmed with acceleration 5E+05 mm/s^2.

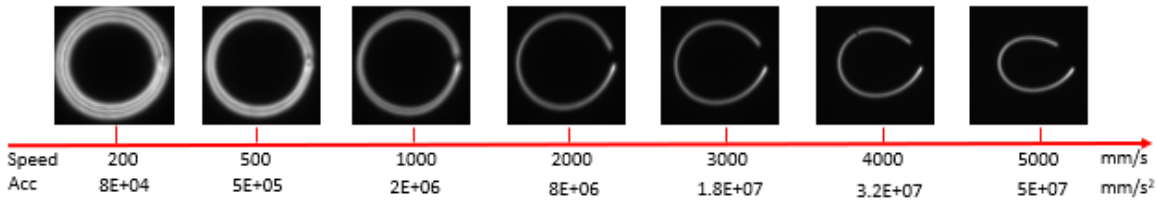

Figure 12. Circles of 1 mm diameter scanned at different speeds. Higher speed requires higher acceleration.

A galvo is a mechanical device; its response is usually slower than the electronics controlling laser power. A time delay (T_{delay}) is introduced into the laser power command to synchronize it with the position. The scan pattern in Figure 13a is designed to calibrate this delay. The images shown in the figure were created using a constant build speed scan strategy [9] with

speed = 1000 mm/s and acceleration = 5E+05 mm/s^2. Figure 13b-e show four images taken at different T_{delay}. If T_{delay} is too short, the laser power is turned on before the laser reaches the designated position (Figure 13b), and if the T_{delay} is too long, the laser power is turned on after the laser reaches the designated position. The images in the figure indicate that T_{delay} = 0.31 ms gives the best intersection for the scan vectors. Theoretically, the optimal T_{delay} can also be calculated from any single scan as long as the velocity profile is known.

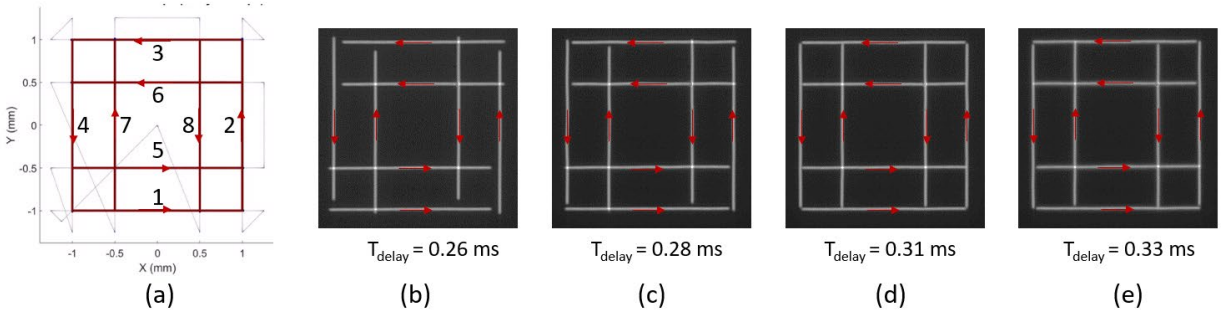

Figure 13. Laser power-position synchronization calibration. (a) Scan strategy designed for the calibration. The numbers indicate the scan sequence. The arrows mark the scan direction. (b) – (e) Images taken at different delay times (T_{delay}).

Conclusion and Future Works

Calibration methods for laser beam size, position, and synchronization are demonstrated. The calibration setup utilizes a low-cost CMOS camera to directly look up the laser beam attenuated by ND filters. The total hardware cost for the setup (camera and ND filters) is only a few hundred dollars (U.S.), and the installation is simple, while the calibration results are comparable to more expensive devices or complicated processes. The demonstration is conducted with a single camera over a small region (size of the CMOS), but it could be easily extended to the whole build plane by mounting the camera at different locations. A base plate with precise multiple camera mounting positions could be manufactured to facilitate this. The calibration procedures outlined in this paper will be further automated to make their execution simple and fast enough to be conducted before each build.

Reference

[1] Badiru AB, Valencia VV, Liu D, editors. Additive Manufacturing Handbook: Product Development for the Defense Industry. 1st ed. CRC Press; 2017. https://doi.org/10.1201/9781315119106.

[2] Land WS. Effective calibration and implementation of galvanometer scanners as applied to direct metal laser sintering, 2014.

[3] Lane B, Moylan S, Yeung H, Neira J, Chavez-Chao J. Quasi-static position calibration of the galvanometer scanner on the additive manufacturing metrology testbed. Gaithersburg, MD: National Institute of Standards and Technology; 2020. https://doi.org/10.6028/NIST.TN.2099.

[4] Yeung H, Lane BM, Donmez MA, Moylan S. In-situ calibration of laser/galvo scanning system using dimensional reference artefacts. CIRP Annals 2020:S0007850620300160. https://doi.org/10.1016/j.cirp.2020.03.016.

[5] Kim FH, Yeung H, Garboczi EJ. Characterizing the effects of laser control in laser powder bed fusion on near-surface pore formation via combined analysis of in-situ melt pool monitoring and X-ray computed tomography. Additive Manufacturing 2021;48:102372. https://doi.org/10.1016/j.addma.2021.102372.
[6] Tang M, Pistorius PC, Beuth JL. Prediction of lack-of-fusion porosity for powder bed fusion. Additive Manufacturing 2017;14:39–48. https://doi.org/10.1016/j.addma.2016.12.001.
[7] Bayat M, Thanki A, Mohanty S, Witvrouw A, Yang S, Thorborg J, et al. Keyhole-induced porosities in Laser-based Powder Bed Fusion (L-PBF) of Ti6Al4V: High-fidelity modelling and experimental validation. Additive Manufacturing 2019;30:100835. https://doi.org/10.1016/j.addma.2019.100835.
[8] Yeung H, Hutchinson, Keely J, Lin, Dong B. Design and Implementation of Laser Powder Bed Fusion Additive Manufacturing Testbed Control Software. Solid Freeform Fabrication 2021: Proceedings of the 32th Annual International Solid Freeform Fabrication Symposium n.d.
[9] Yeung H, Lane BM, Donmez MA, Fox JC, Neira J. Implementation of Advanced Laser Control Strategies for Powder Bed Fusion Systems. Procedia Manufacturing 2018;26:871–9. https://doi.org/10.1016/j.promfg.2018.07.112.
[10] Wei JC, Zhang GY, Chen Y, Yan XT. Design of a Communication Interface between the Controller and the Galvanometer. AMM 2014;527:269–72. https://doi.org/10.4028/www.scientific.net/AMM.527.269.